

# Anomalous Higgs couplings in $e\gamma$ collision with initial beam and final state polarizations

İnanç Şahin\*

*Department of Physics, Faculty of Sciences,  
Ankara University, 06100 Tandogan, Ankara, Turkey*

## Abstract

We investigate the constraints on the anomalous  $WWH$  couplings through the process  $e^-\gamma \rightarrow \nu_e W^- H$ . Considering incoming beam polarizations and the longitudinal and transverse polarization states of the final  $W$  boson we find 95% confidence level limits on the anomalous coupling parameters with an integrated luminosity of  $500 \text{ fb}^{-1}$  and  $\sqrt{s} = 1 \text{ TeV}$  energy. We show that initial beam and final state polarizations highly improve the sensitivity limits of the anomalous coupling parameters  $b_W$  and  $\beta_W$ .

PACS numbers: 12.15.Ji, 12.60.Fr, 13.88.+e

---

\*isahin@science.ankara.edu.tr

## I. INTRODUCTION

Standard Model (SM) of particle physics has been proved to be successful in the energy scale of the present colliders. Experimental results obtained from recent experiments at CERN LEP and Fermilab Tevatron confirms the  $SU(3)_C \times SU(2)_L \times U(1)_Y$  gauge structure of SM. However Higgs boson which is crucial for electroweak symmetry breaking and mass generation has not been observed and one of the main goals of future experiments is to pursue its trace. Although the exact value of the Higgs mass is unknown there are experimental bounds for it. Direct searches from ALEPH, DELPHI, L3 and OPAL collaborations at CERN LEP provide a lower bound on the Higgs mass of  $m_H > 114.4$  GeV [1]. Indirect experimental bounds for the Higgs mass are obtained from fits to precision measurements of electroweak observables. The current best fit value sets an upper bound of  $m_H < 186$  GeV [2].

If a Higgs boson is detected at future TeV scale colliders it will be crucial to test its couplings to the SM particles. Precision measurements of Higgs couplings may give us some hints for new physics beyond the SM. It is argued that CERN LHC has a potential to search for the Higgs boson in the entire mass range allowed. In case it is found at CERN LHC, precision measurements of its couplings to the SM particles can be obtained at future linear  $e^+e^-$  colliders. After linear  $e^+e^-$  colliders are constructed its operating modes of  $e\gamma$  and  $\gamma\gamma$  are expected to be designed [3]. Real gamma beam is obtained through Compton backscattering of laser light off linear electron beam where most of the photons are produced at the high energy region. The luminosities for  $e\gamma$  and  $\gamma\gamma$  collisions turn out to be of the same order as the one for  $e^+e^-$  [4], so the cross sections for photoproduction processes with real photons are considerably larger than the virtual photon case. Polarizability of real gamma beam is an additional advantage for polarized beam experiments. Therefore  $e\gamma$  and  $\gamma\gamma$  collisions should be discussed as complementary to  $e^+e^-$  collisions.

In this work we analyzed anomalous WWH vertex in the  $e\gamma$  collision. We consider the process  $e^-\gamma \rightarrow \nu_e W^- H$ . This process isolates WWH vertex and gives us the opportunity to study WWH vertex independent from ZZH. On the other hand in  $e^+e^-$  collisions, observables depending on WWH also receive contributions from the ZZH and it is very difficult to dissociate WWH from ZZH [5].

Anomalous WWH couplings can be investigated in a model independent way by means

of effective Lagrangian approach [5, 6, 7, 8]. In writing effective operators we employ the formalism of [5, 8]. Imposing Lorentz invariance and gauge invariance and retaining up to dimension six operators in the effective Lagrangian, the most general coupling structure is expressed as,

$$\Gamma_{\mu\nu}^V = i\tilde{g}_V \left[ a_V g_{\mu\nu} + \frac{b_V}{m_V^2} (k_{2\mu} k_{1\nu} - g_{\mu\nu} k_1 \cdot k_2) + \frac{\beta_V}{m_V^2} \epsilon_{\mu\nu\alpha\beta} k_1^\alpha k_2^\beta \right] \quad (1)$$

with

$$\tilde{g}_W = g_W m_W, \quad \tilde{g}_Z = \frac{g_W m_W}{\cos^2 \theta_W}, \quad g_W = \frac{g_e}{\sin \theta_W} \quad (2)$$

where  $k_1^\mu$  and  $k_2^\mu$  represent the momentum of two W or Z boson (V=W, Z). For a convention we assume that all the momenta are outgoing from the vertex. Within the standard model at tree level, the couplings are given by  $a_V = 1$ ,  $b_V = 0$  and  $\beta_V = 0$ .

In the literature there have been several studies for anomalous WWH couplings. The LHC will start operating soon. Anomalous gauge couplings of the Higgs boson have been studied at LHC via the weak-boson scattering [9] and vector boson fusion [10] processes. There have been great amount of work on anomalous WWH couplings which focus on future linear  $e^+e^-$  collider and its  $e\gamma$  and  $\gamma\gamma$  modes. Anomalous WWH couplings have been analyzed through the processes  $e^+e^- \rightarrow f\bar{f}H$  [5, 7],  $e^+e^- \rightarrow W^+W^-\gamma$  [11],  $e^-\gamma \rightarrow \nu_e W^- H$  [8] and  $\gamma\gamma \rightarrow WWWW$  [12]. In ref.[8] authors ignore quadratic anomalous coupling terms in the cross section calculations, they retain contributions only up to the lowest nontrivial order. This is reasonable due to the higher dimensional nature of their origin. On the other hand these quadratic terms generally have a higher momentum dependence than linear terms and may have a significant contribution at high energies. Therefore we will consider all anomalous terms in our tree level cross section calculations.

As in ref.[8] we take into account of initial electron and photon polarizations before Compton backscattering. Furthermore we take into account of initial electron beam polarization which takes part in the subprocess and also the final state polarizations of W boson. We will show that these polarization configurations which haven't been considered in ref.[8], leads to a significant amount of improvement in the sensitivity limits.

## II. POLARIZED CROSS SECTIONS

The process  $e^-\gamma \rightarrow \nu_e W^- H$  takes part as a subprocess in the  $e^+e^-$  collision. Real gamma beam which enters the subprocess is obtained through Compton backscattering of laser light off linear electron or positron beam.

The spectrum of backscattered photons in connection with helicities of initial laser photon and electron is given by [4]:

$$f_{\gamma/e}(y) = \frac{1}{g(\zeta)} \left[ 1 - y + \frac{1}{1-y} - \frac{4y}{\zeta(1-y)} + \frac{4y^2}{\zeta^2(1-y)^2} + \lambda_0 \lambda_e r \zeta (1-2r)(2-y) \right] \quad (3)$$

where

$$g(\zeta) = g_1(\zeta) + \lambda_0 \lambda_e g_2(\zeta) \quad (4)$$

$$g_1(\zeta) = \left( 1 - \frac{4}{\zeta} - \frac{8}{\zeta^2} \right) \ln(\zeta + 1) + \frac{1}{2} + \frac{8}{\zeta} - \frac{1}{2(\zeta + 1)^2}$$

$$g_2(\zeta) = \left( 1 + \frac{2}{\zeta} \right) \ln(\zeta + 1) - \frac{5}{2} + \frac{1}{\zeta + 1} - \frac{1}{2(\zeta + 1)^2} \quad (5)$$

Here  $r = y/[\zeta(1-y)]$  and  $\zeta = 4E_e E_0/M_e^2$ .  $E_0$  and  $\lambda_0$  are the energy and helicity of initial laser photon and  $E_e$  and  $\lambda_e$  are the energy and the helicity of initial electron beam before Compton backscattering.  $y$  is the fraction which represents the ratio between the scattered photon and initial electron energy for the backscattered photons moving along the initial electron direction. Maximum value of  $y$  reaches 0.83 when  $\zeta = 4.8$  in which the backscattered photon energy is maximized without spoiling the luminosity.

Backscattered photons are not in fixed helicity states their helicities are described by a distribution :

$$\xi(E_\gamma, \lambda_0) = \frac{\lambda_0(1-2r)(1-y+1/(1-y)) + \lambda_e r \zeta [1 + (1-y)(1-2r)^2]}{1-y+1/(1-y) - 4r(1-r) - \lambda_e \lambda_0 r \zeta (2r-1)(2-y)} \quad (6)$$

The helicity dependent differential cross section for the subprocess can be connected to initial laser photon helicity  $\lambda_0$  and initial electron beam polarization  $P_e$  through the formula,

$$\begin{aligned}
& d\hat{\sigma}(\lambda_0, P_e; \lambda_W) \\
&= \frac{1}{4}(1 - P_e) [(1 + \xi(E_\gamma, \lambda_0))d\hat{\sigma}(+, L; \lambda_W) + (1 - \xi(E_\gamma, \lambda_0))d\hat{\sigma}(-, L; \lambda_W)] \\
&+ \frac{1}{4}(1 + P_e) [(1 + \xi(E_\gamma, \lambda_0))d\hat{\sigma}(+, R; \lambda_W) + (1 - \xi(E_\gamma, \lambda_0))d\hat{\sigma}(-, R; \lambda_W)] \quad (7)
\end{aligned}$$

Here  $d\hat{\sigma}(\lambda_\gamma, \sigma; \lambda_W)$  is the helicity dependent differential cross section in the helicity eigenstates;  $\sigma : L, R$ ,  $\lambda_\gamma = +, -$  and  $\lambda_W = +, -, 0$ . It should be noted that  $P_e$  and  $\lambda_e$  refer to different beams.  $P_e$  is the electron beam polarization which enters the subprocess but  $\lambda_e$  is the polarization of initial electron beam before Compton backscattering.

The integrated cross section over the backscattered photon spectrum is,

$$d\sigma(\lambda_0, P_e; \lambda_W) = \int_{y_{min}}^{0.83} f_{\gamma/e}(y) d\hat{\sigma}(\lambda_0, P_e; \lambda_W) dy \quad (8)$$

where,  $y_{min} = \frac{(m_z + m_H)^2}{s}$ .

The process  $e^- \gamma \rightarrow \nu_e W^- H$  is described by three tree-level diagrams Fig.1. Each of the diagram contains anomalous WWH vertex. The helicity amplitudes have been calculated using vertex amplitude techniques derived in ref.[13] and the phase space integrations have been performed by GRACE [14] which uses a Monte Carlo routine.

In our calculations we choose to work with a Higgs boson of mass 120 GeV which is compatible with current mass bounds. we accept that initial electron beam polarizability is  $|\lambda_e|, |P_e|=0.8$ . To see the influence of initial beam polarization, energy distributions of backscattered photons  $f_{\gamma/e}$  are plotted for  $\lambda_e \lambda_0=0, -0.8$  and  $+0.8$  in Fig.2. We see from the figure that backscattered photon distribution is very low at high energies in  $\lambda_e \lambda_0=+0.8$ . Therefore we will only consider the case  $\lambda_e \lambda_0 < 0$  in the cross section calculations.

One can see from Fig.3-5 the influence of the initial state polarizations on the deviations of the total cross sections from their SM value. In Fig.3 initial polarization configurations  $(\lambda_e, \lambda_0, P_e) = (+0.8, -1, \mp 0.8)$  are omitted since they coincide with  $(\lambda_e, \lambda_0, P_e) = (-0.8, +1, \mp 0.8)$ . We see from Fig.3-5 that cross section is very sensitive to  $P_e$ . This is reasonable due to  $V-A$  structure of the  $W e \nu_e$  vertex in the Feynman diagrams. Deviation of the cross section from its SM value reaches its maximum at the  $(\lambda_e, \lambda_0, P_e) = (-0.8, +1, -0.8)$  polarization configuration. In Fig.6-8 we plot the total cross section as a function of anomalous parameters for various final state polarizations. In these figures TR and LO stand for

"transverse" and "longitudinal" respectively. We see from these figures that cross section is very small in the longitudinal polarization configuration. On the other hand longitudinal polarization remarkably improves the deviations from the SM at the positive values of the parameter  $b_W$ . For instance in Fig.7 longitudinal cross section increases by a factor of 12 as  $b_W$  increases from 0 to 0.21. But this increment is only a factor of 1.4 for the unpolarized case. The reason for this comes from the fact that longitudinal cross section has a symmetric behavior in the positive and negative intervals of the parameter but unpolarized graph shift a little to the right. Longitudinal polarization also improves the deviations from the SM at both positive and negative values of  $\beta_W$ .

Angular distributions of the Higgs boson for unpolarized and longitudinally polarized cross sections are given in Fig.9 and Fig.10. In the figures  $\theta_H$  is the angle between the outgoing Higgs boson and the incoming electron in the center of mass frame of  $e^+e^-$ . Angular distributions for other polarization configurations are very similar to the unpolarized cross section. So we won't give them in the paper. One can see from Fig.10 that deviation of the differential cross section from its SM value is larger in the negative interval of  $\theta_H$ .

### III. LIMITS ON THE ANOMALOUS COUPLING PARAMETERS

For a concrete result we have obtained 95% C.L. limits on the anomalous coupling parameters  $a_W$ ,  $b_W$  and  $\beta_W$  using  $\chi^2$  analysis at  $\sqrt{s} = 1$  TeV and integrated luminosity  $L_{int} = 500$  fb $^{-1}$  without systematic errors. In our calculations we choose to work with a Higgs boson of mass 120 GeV. Therefore the dominant decay mode should be  $H \rightarrow b\bar{b}$  with a branching ratio  $B_H \approx 0.9$ .

We assume that W polarization can be measured. Indeed angular distribution of the W decay products has a clear correlation with the helicity states of the W boson. Therefore we consider the case in which W momentum is reconstructible. We restrict ourselves to  $W \rightarrow q\bar{q}$  decay channel with a branching ratio  $B_W \approx 0.68$ . The number of events are given as  $N = EB_W B_H L_{int} \sigma$  where  $E$  is the b-tagging efficiency and it is taken to be 0.7 as ref.[5, 8].

Limits on the anomalous WWH couplings are given in Table I for various initial and final polarization configurations. In the table,  $(\lambda_0, \lambda_e, P_e) = (0, 0, 0)$  is for unpolarized initial beams and TR+LO represents unpolarized W boson. We take into account of  $(\lambda_0, \lambda_e, P_e) =$

(+1, -0.8, -0.8) initial polarization configuration which gives the largest deviation from the SM Fig.3-5. It can be seen from Fig.10 that deviation of the differential cross section from its SM value is larger in the negative interval of  $\theta_H$ . So we impose a restriction  $\cos \theta_H < 0$  on longitudinal polarization configuration to improve the limits. We represent these restricted limits with a superscript " \* ". We see from Table I that polarization leads to a significant improvement in the upper bound of  $b_W$ . Polarization improve the upper bound of  $b_W$  a factor of 7.4. This improvement factor become 9.3 when we consider  $\cos \theta_H < 0$  restriction. Polarization improve both upper and lower bounds of  $\beta_W$ . Improvement factors for upper and lower bounds are same and equal to 2.2. Final state polarizations do not improve the lower bound of  $b_W$ . But initial polarizations improve the lower bound of  $b_W$  a factor of 1.7.

- 
- [1] R. Barate *et al.*, Phys. Lett. **B 565**, 61 (2003).
  - [2] LEP Electroweak Working Group, <http://lepewwg.web.cern.ch/LEPEWWG/>.
  - [3] C. Akerlof, Ann Arbor Report No. UM HE 81-59 (1981);  
T.L. Barklow, in Proceedings of the 1990 Summer Study on Research Directions for the Decade (Snowmass, Colorado, 1990), and SLAC Report No. SLAC-PUB-5364 (1990);  
J. A. Aguilar-Saavedra *et al.* , TESLA Technical Design Report Part III, DESY-2001-011.
  - [4] I.F. Ginzburg *et al.*, Nucl. Instrum. Methods **205**, 47 (1983); *ibid.* **219**, 5 (1984).
  - [5] S.S. Biswal, D. Choudhury, R.M. Godbole and R.K. Singh, Phys. Rev. **D73**, 035001 (2006).
  - [6] M.C. Gonzalez-Garcia, Int. J. Mod. Phys. **A14**, 3121 (1999).
  - [7] V. Barger, T. Han, P. Langacker, B. McElrath and P. Zerwas, Phys. Rev. **D67**, 115001 (2003).
  - [8] D. Choudhury and Mamta, Phys. Rev. **D74**, 115019 (2006).
  - [9] H.-J. He, Y.-P. Kuang, C.-P. Yuan and B. Zhang, Phys. Lett. **B 554**, 64 (2003);  
B. Zhang, Y.-P. Kuang, H.-J. He and C.-P. Yuan, Phys. Rev. **D 67**, 114024 (2003).
  - [10] V. Hankele, G. Klänke, D. Zeppenfeld and T. Figy, Phys. Rev. **D 74**, 095001 (2006).
  - [11] M.C. Gonzalez-Garcia, S. M. Lietti and S. F. Novaes, Phys. Rev. **D59**, 075008 (1999).
  - [12] T. Han, Y-P. Kuang and B. Zhang, Phys. Rev. **D 73**, 055010 (2006).
  - [13] A. Ballestrero and E. Maina, Phys. Lett. **B350**, 225(1995).
  - [14] T. Kaneko in *New Computing Techniques in Physics Research*, edited by D. Perret-Gallix, W. Wojcik (Edition du CNRS, Paris, 1990); MINAMI-TATEYA Group, KEK Report No. 92-19,

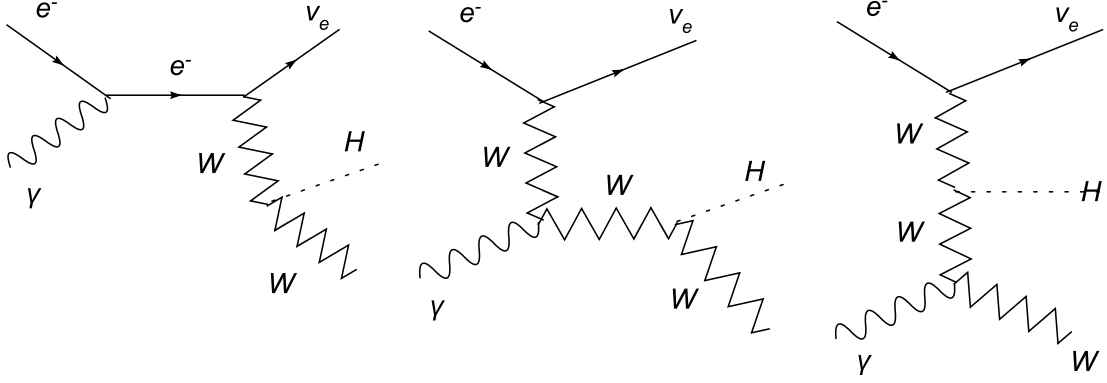


FIG. 1: Tree-level Feynman diagrams for  $e^- \gamma \rightarrow \nu_e W^- H$ .

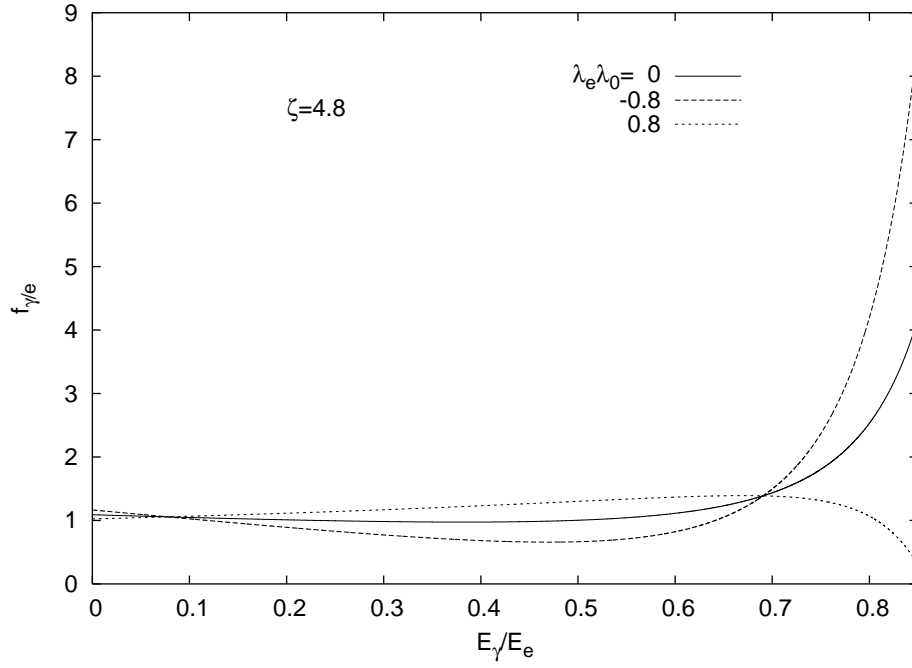


FIG. 2: Energy distribution of backscattered photons for  $\lambda_e \lambda_0 = 0, -0.8, 0.8$ .

1993; F. Yuasa *et al.*, Prog. Theor. Phys. Suppl. **138** 18 (2000).



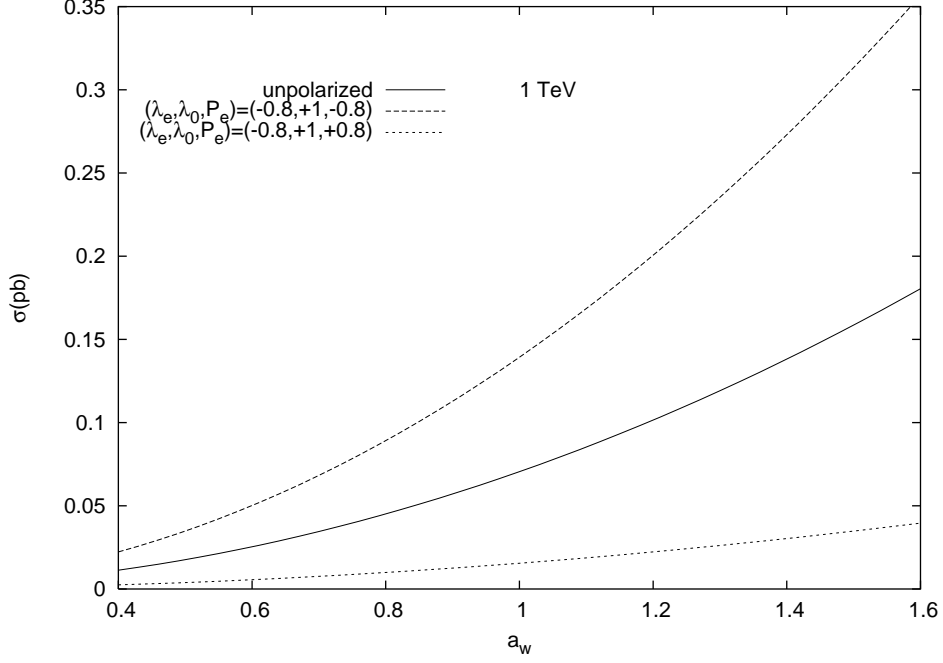


FIG. 3: The integrated total cross section of  $e^- \gamma \rightarrow \nu_e W^- H$  as a function of anomalous coupling  $a_W$ . The legends are for initial beam polarizations.  $\sqrt{s} = 1 TeV$ .

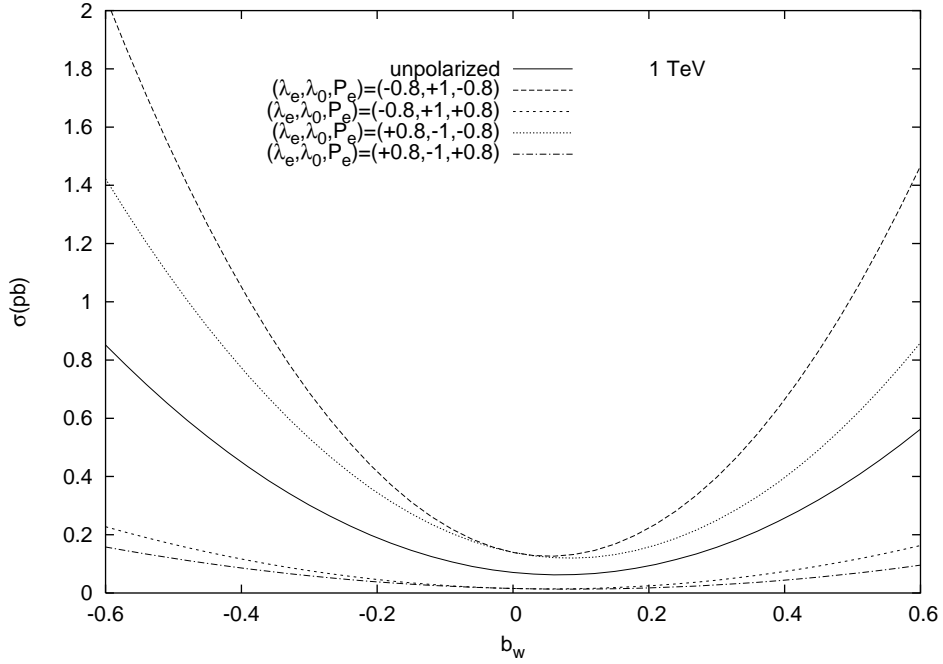


FIG. 4: The integrated total cross section of  $e^- \gamma \rightarrow \nu_e W^- H$  as a function of anomalous coupling  $b_W$ . The legends are for initial beam polarizations.  $\sqrt{s} = 1 TeV$ .

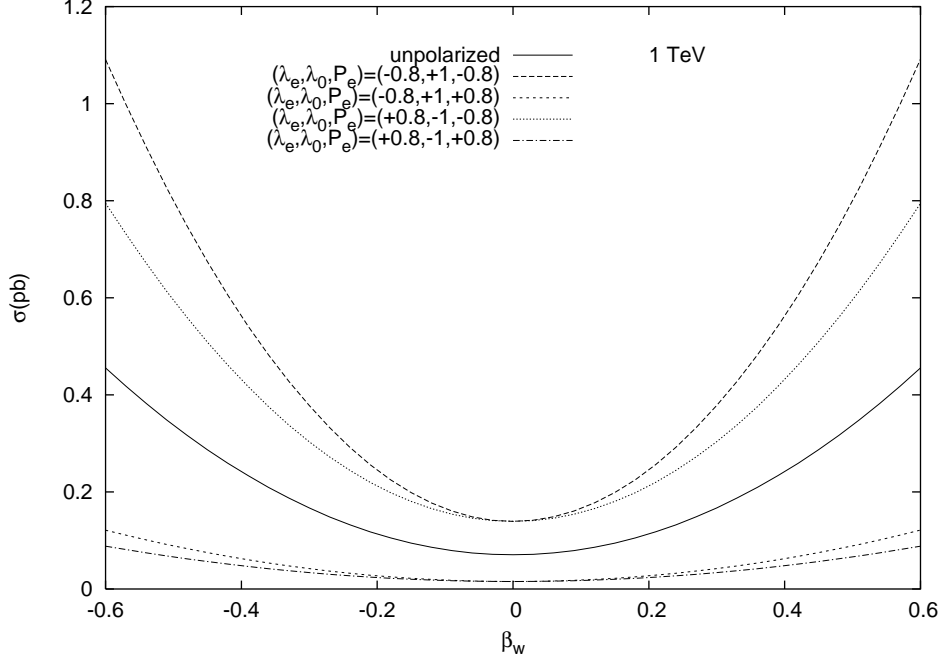


FIG. 5: The integrated total cross section of  $e^- \gamma \rightarrow \nu_e W^- H$  as a function of anomalous coupling  $\beta_W$ . The legends are for initial beam polarizations.  $\sqrt{s} = 1 \text{ TeV}$ .

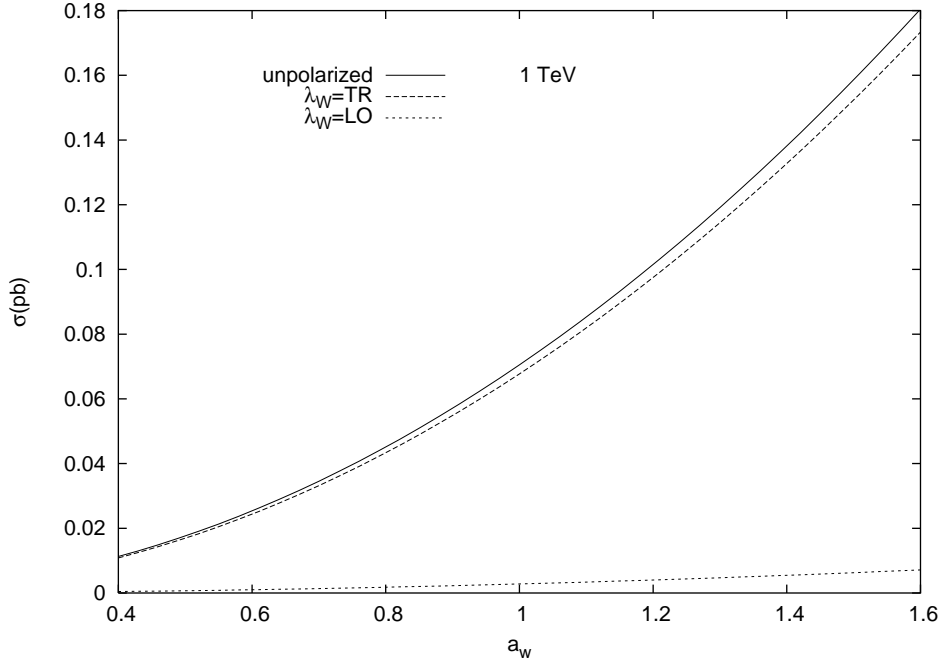


FIG. 6: The integrated total cross section of  $e^- \gamma \rightarrow \nu_e W^- H$  as a function of anomalous coupling  $a_W$ . The legends are for final state polarizations.  $\sqrt{s} = 1 \text{ TeV}$ .

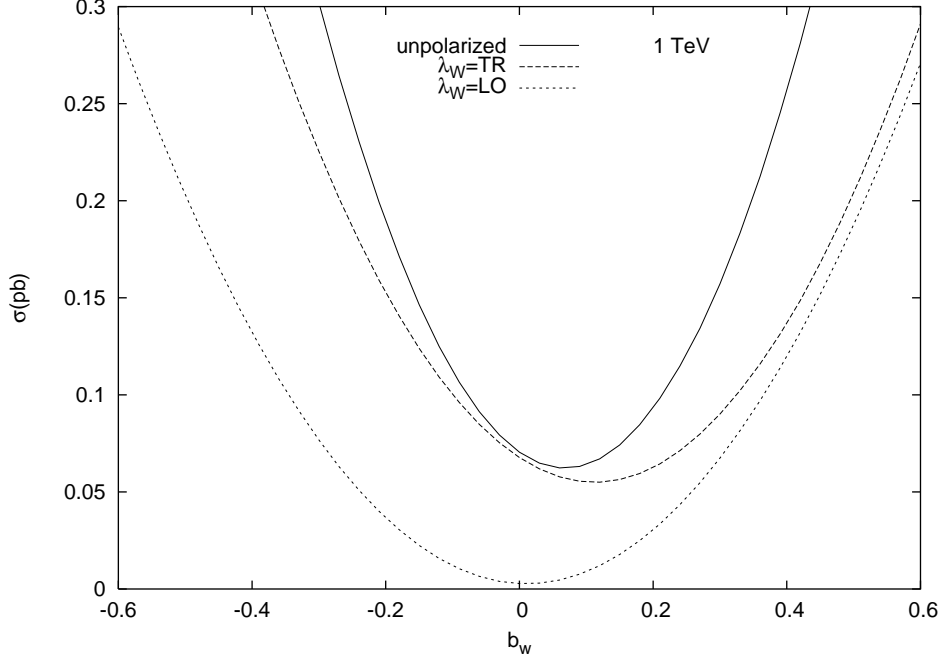


FIG. 7: The integrated total cross section of  $e^-\gamma \rightarrow \nu_e W^- H$  as a function of anomalous coupling  $b_W$ . The legends are for final state polarizations.  $\sqrt{s} = 1TeV$ .

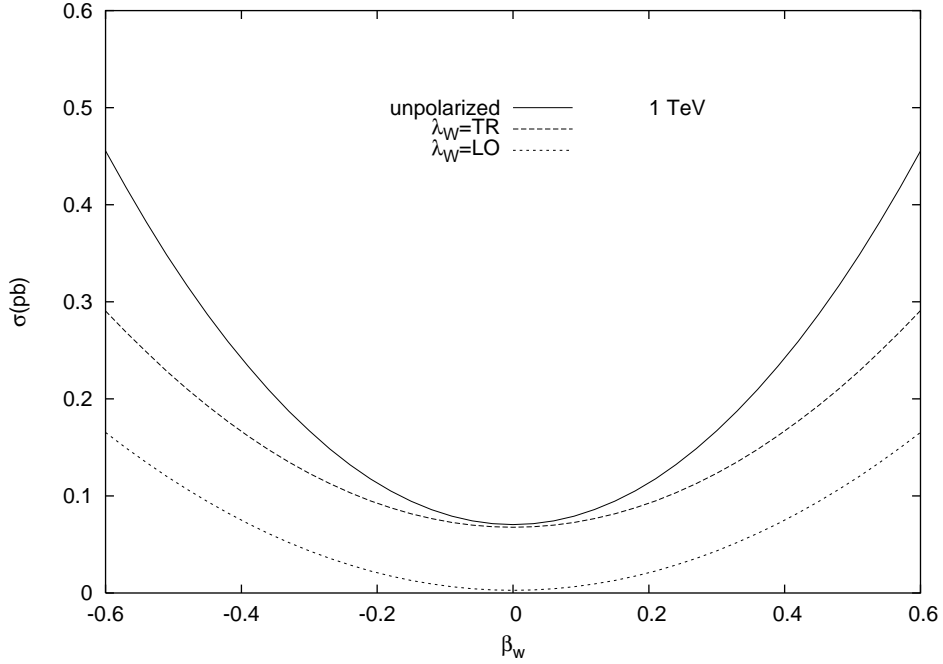


FIG. 8: The integrated total cross section of  $e^-\gamma \rightarrow \nu_e W^- H$  as a function of anomalous coupling  $\beta_W$ . The legends are for final state polarizations.  $\sqrt{s} = 1TeV$ .

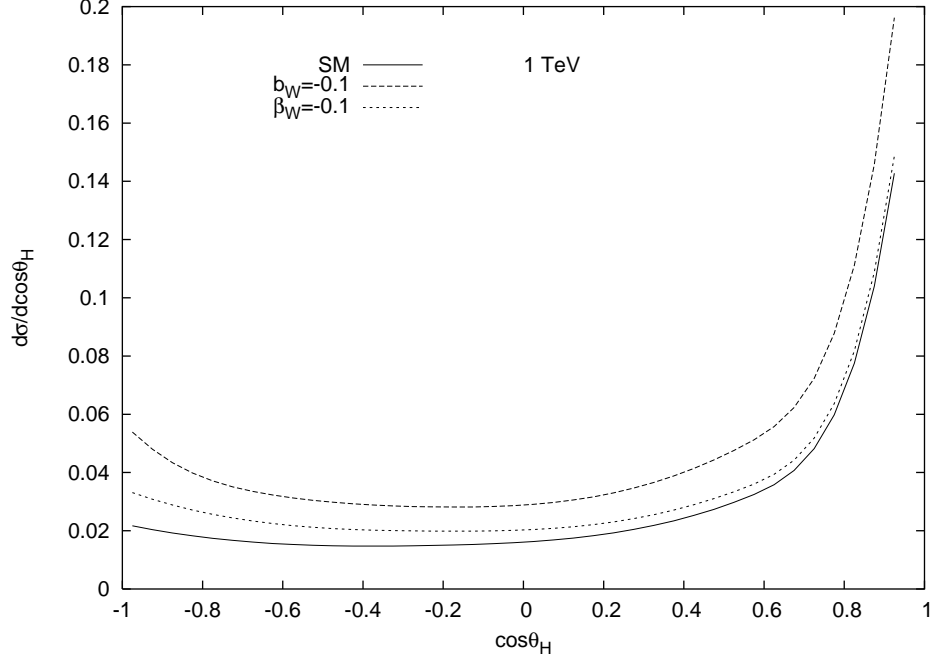


FIG. 9: Angular distributions of the Higgs boson in the center of mass frame of  $e^+e^-$  for unpolarized beams.  $\theta_H$  is the angle between the outgoing Higgs boson and the incoming electron.

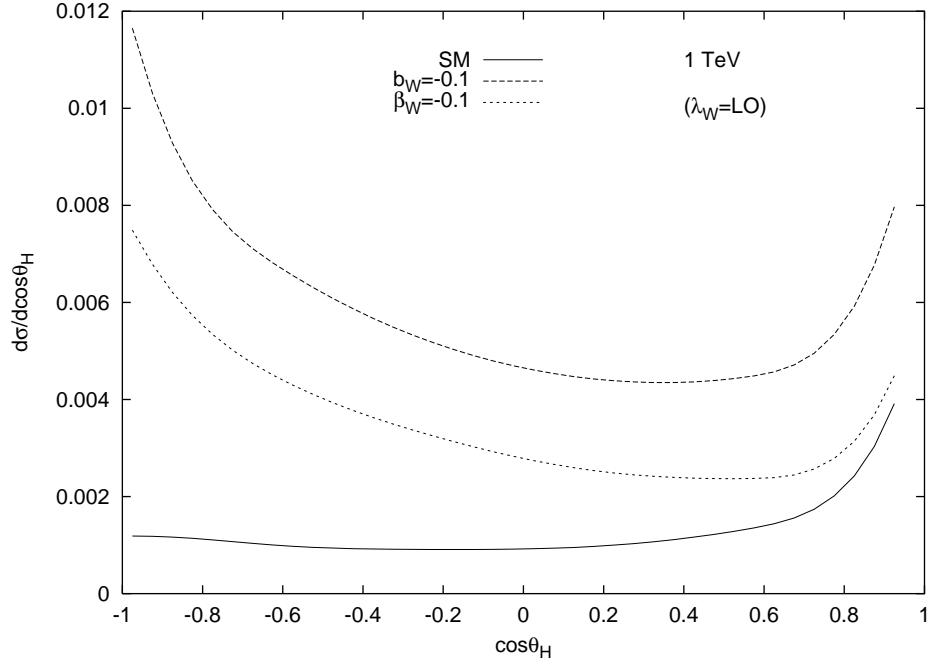


FIG. 10: Angular distributions of the Higgs boson in the center of mass frame of  $e^+e^-$  for longitudinal polarization state of the final W.

TABLE I: Sensitivity of the  $e\gamma$  collision to anomalous  $WWH$  couplings at 95% C.L. for  $\sqrt{s} = 1$  TeV and  $L_{int} = 500 \text{ fb}^{-1}$ . The effects of final state W boson polarization and initial beam polarizations are shown in each row. Superscript " \* " represents the restriction  $\cos \theta_H < 0$  in the phase space.

$\lambda_0$	$\lambda_e$	$P_e$	$\lambda_W$	$a_W$	$b_W$	$\beta_W$
0	0	0	$TR + LO$	(0.992, 1.008)	(-0.005, 0.140)	(-0.033, 0.033)
0	0	0	$TR$	(0.992, 1.008)	(-0.005, 0.230)	(-0.043, 0.043)
0	0	0	$LO$	(0.960, 1.040)	(-0.010, 0.030)	(-0.023, 0.023)
0	0	0	$LO^*$	(0.931, 1.065)*	(-0.011, 0.022)*	(-0.020, 0.020)*
+1	-0.8	-0.8	$TR + LO$	(0.995, 1.006)	(-0.003, 0.111)	(-0.024, 0.024)
+1	-0.8	-0.8	$TR$	(0.995, 1.006)	(-0.003, 0.205)	(-0.033, 0.033)
+1	-0.8	-0.8	$LO$	(0.970, 1.030)	(-0.007, 0.019)	(-0.015, 0.015)
+1	-0.8	-0.8	$LO^*$	(0.953, 1.047)*	(-0.008, 0.015)*	(-0.014, 0.014)*